J. Fluid Mech. (1969), *vol.* 37, *part* 4, *pp.* 799–825
Printed in Great Britain

Peristaltic pumping with long wavelengths at low Reynolds number

By A. H. SHAPIRO, M. Y. JAFFRIN AND S. L. WEINBERG
Department of Mechanical Engineering, Massachusetts Institute of Technology

(Received 10 September 1968 and in revised form 23 January 1969)

Pumping by means of an infinite train of peristaltic waves is investigated under conditions for which the relevant Reynolds number is small enough for inertial effects to be negligible and the wavelength to diameter ratio is large enough for the pressure to be considered uniform over the cross-section. Theoretical results are presented for both plane and axisymmetric geometries, and for amplitude ratios ranging from zero to full occlusion. For a given amplitude ratio, the theoretical pressure rise per wavelength decreases linearly with increasing time-mean flow. An experiment with a quasi-two-dimensional apparatus confirmed the theoretical values.

Calculations of the detailed fluid motions reveal that under many conditions of operation the net time-mean flow is the algebraic difference between a forward time-mean flow in the core of the tube and a backward ('reflux') time-mean flow near the periphery. The percentage of reflux flow can be very high. This reflux phenomenon is probably of physiologic significance in the functioning of the ureter and the gastro-intestinal system. A second fluid-mechanical peculiarity with physiological implications is that of 'trapping': under certain conditions an internally circulating bolus of fluid, lying about the axis, is transported with the wave speed as though it were trapped by the wave.

1. Introduction

1.1. *Object and scope*

This paper is concerned with the fluid mechanics of peristaltic pumping under conditions for which (i) the length of the peristaltic wave is large compared with the channel width, and (ii) the appropriate Reynolds number is sufficiently small for the flow to be considered inertia-free. These conditions appear to be reasonably well met in the human ureter and, to a lesser extent, in the gastro-intestinal tract and in mechanical roller pumps using viscous fluids.

In § 3, the gross pumping characteristics of an infinite wave-train are developed for the two-dimensional plane and axisymmetric cases. A comparison of the theory with an approximately two-dimensional plane experiment is given in § 4. In §§ 5 and 6, the details of the fluid motions are studied for plane and axisymmetric flow, respectively. Two surprising phenomena are discovered, described here as reflux and trapping.

1.2. *An elementary view of how a peristaltic pump works*

Figure 1 gives a simple physical picture of how a peristaltic pump works; it also suggests conclusions that are correct more generally.

The upper drawing (laboratory frame) shows a long tube closed at both ends, in which a peristaltic wave of contraction is produced by moving a sliding cuff to the right at speed c. Because of the closures at the two ends, there is no flow in either large cross-section. In the wave frame of reference (lower drawing), which moves rightwards with the speed c relative to the laboratory frame, the

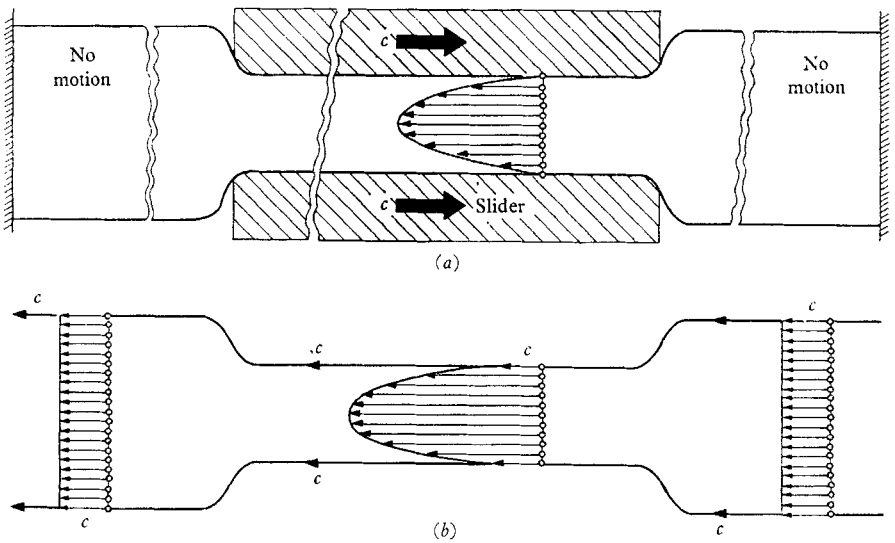

FIGURE 1. Schematic to illustrate mechanism of peristaltic pumping. (*a*) As seen in laboratory frame (unsteady). (*b*) As seen in wave frame (steady).

wave-form appears stationary. Also, the walls move leftwards with the speed c, and there is a uniform plug flow to the left, of speed $-c$, in the large cross-sections. To conserve volume flow of an incompressible fluid, the average leftwards velocity in the contracted section must exceed c. Assuming for the moment that the flow is viscous and inertia-free, the velocity profile in the contracted section must be parabolic, with velocity $-c$ at the walls. There is no pressure gradient in the large cross-sections, but the pressure falls from right to left in the contracted section, owing to viscous losses.

This same pressure gradient exists in the laboratory frame. Thus the peristaltic wave tends to produce a rising pressure in the direction of the wave. In the laboratory frame, the longitudinal velocity distribution in the contracted section is a leftwards Poiseuille flow, with zero longitudinal speed at the walls.

If the closures are removed, there will be an additional flow, the amount depending on the end pressures imposed. During operation as a pump, fluid will be transported rightward through the larger sections, and the leftward flow in the contracted section will be reduced, as compared with the closed-end case.

The associated Poiseuille viscous losses will reduce the pressure rise produced by the peristaltic motion.

Two conclusions, applicable to more general wave-forms, can be drawn from the foregoing arguments. (i) Dissipation is an essential feature of peristaltic pumping. Without viscous effects, the flow in the contracted section would be a plug flow and would have no associated pressure drop. Alternatively, Bernoulli's integral, when applied to an assumed steady-state inviscid flow observed in the wave frame, would show no net pressure change across the contraction wave. (ii) As seen in the laboratory frame, the usual condition in a peristaltic wave is that the fluid in contracted sections moves opposite to the wave direction, and the fluid in enlarged sections moves in the same direction as the wave.

1.3. *Related work*

For infinite wave-train, the dimensionless parameters of the problem are: (*a*) a wave-number, a/λ, where a is the mean half-width of the passage (plane geometry) or the mean radius (axisymmetric geometry), and λ is the wavelength; (*b*) an amplitude ratio, $\phi \equiv b/a$, where b is the half-amplitude of a peristaltic wave; (*c*) a Reynolds number, R, which we show later best measures small inertia effects when defined as $R \equiv (ac/\nu).(a/\lambda)$; (*d*) a dimensionless time-mean flow, e.g. $\theta \equiv \bar{Q}/bc$ for the plane case, where $\bar{Q}$ is the time-mean flow observed in the laboratory frame. For fixed values of the first three, the fourth may have any value, depending upon the pressure rise against which the pump works.

Table 1 summarizes the assumptions in the theoretical investigations of Burns & Parkes (1967), of Hanin (1968) and of Fung & Yih (1969), compared with the assumptions of the present paper. All deal with an infinite train of sinusoidal waves. Burns & Parkes develop their solution as an expansion in ascending powers of ϕ. Explicit algebraic results do not emerge, and numerical calculations are necessary. In some examples, these are carried to order ϕ^4.

	Burns & Parkes	Hanin	Fung & Yih	Present paper
Geometry	Plane axisym.	Plane	Plane	Plane axisym.
Reynolds number, R	Zero	Arbitrary	Arbitrary	Zero
Wave-number, a/λ	Arbitrary	Zero	Arbitrary	Zero
Amplitude ratio, ϕ	Small†	Small†	Small†	Arbitrary

† Solution is expressed in ascending powers of ϕ.

TABLE 1

Hanin's solution is restricted by the additional assumption that the mean pressure gradient is zero. This is equivalent to restricting θ to a single value for each value of ϕ. Hanin's solution is also expressed as an expansion in ascending powers of ϕ. He gives some explicit results valid to first-order in ϕ for the oscillatory flow and to second-order for the mean flow. Fung & Yih, also using an expansion in ascend-

ing powers of ϕ, give results up to order ϕ^2. The present solution is limited to small R (inertia-free case), and to small a/λ (large λ). On the other hand, ϕ is arbitrary, and many important results are given in closed form.

1.4. *Physiologic data for the ureter*

The geometric and kinematic properties of the ureter are not well established. They vary greatly among individuals, and from time to time (see Boyarsky 1964; Campbell 1963; Kiil 1957; Maksimov & Bloom 1957; Narath 1951). Although we have insufficient knowledge of the minimum cross-sectional shape and dimensions during peristalsis, enough seems to be known to set the context of a fluid-dynamic analysis. Table 2 shows the ranges of the variables for the human ureter. The cross-sectional shape varies from nearly round, when fully distended, to roughly star-shaped, with flat quasi-two-dimensional lobes, when contracted.

Length	30 cm
Inside diameter	from 0·01 cm (in doubt) to 0·5 cm (extreme!)
Wave speed	from 1 cm/s to 6 cm/s
Frequency	several waves per minute
Wavelength	from 1 cm to 15 cm

TABLE 2

In the theoretical model defined below, the purpose is not to represent exactly the functioning of the ureter, but rather to explore in as simple a way as possible the fluid-mechanical phenomena inherent in peristalsis. Presumably the results of the simple model have some relevance to ureter function.

2.5. *Theoretical model*

The rationalization of the theoretical model given below is based on order-of-magnitude physical analysis. In appendices A and B, the implications of the assumptions regarding a/λ and R are more clearly and fully developed by normalization and order-of-magnitude analysis of the differential equations.

(i) *Infinite wavelength.* The ratio of width to wavelength is assumed to be small, i.e. $a/\lambda \ll 1$. If, for the ureter, we take $a \cong 0{\cdot}1$ and $\lambda \cong 5$ cm, then $a/\lambda \cong 1/50$. Thus the slope of the wall is very small, and it may be shown that the transverse velocities and pressure gradients are small compared with the longitudinal values. This simplifies the solution, because one may assume that the pressure is instantaneously uniform over each cross-section.

(ii) *Inertia-free flow.* We are interested in the case where the peristaltic wave acts as a pump, i.e. it produces a pressure rise in the direction of the mean flow. As shown later, under these conditions the longitudinal velocity as observed in the wave frame is of order c. Thus the leading viscous term in the equation of motion, $\mu \partial^2 u/\partial y^2$, is of order $\mu c/a^2$, at least when viscous effects are strong and not confined to thin boundary layers, where x, y are co-ordinates in the wave frame, u, v are the velocity components, and μ is viscosity. Since $\partial u/\partial x$ is of order

c/λ, the typical inertia term $\rho u\,\partial u/\partial x$ is of order $\rho c^2/\lambda$, for density ρ. Thus the ratio of inertial to viscous forces is of order $(ca/\nu)\,(a/\lambda)$, where ν is the kinematic viscosity. This is the appropriate R for cases with small inertial effects, as confirmed in appendices A and B. In the model we assume that R is so small that the inertia terms in the equation of motion may be ignored.

If, for the human ureter, we take $c \cong 3$ cm/s, $a \cong 0{\cdot}1$ cm, $\nu \cong 0{\cdot}007$ cm^2/s and $\lambda \cong 5$ cm, then $R \cong 1$. This is so small that one may apply an inertia-free theory; indeed, as shown in § 3.2, the inertia-free theory should be quite accurate. The assumptions of infinite wavelength and inertia-free flow, taken together, are equivalent to the assumption that the flow is instantaneously of Poiseuille type at each local cross-section.

(iii) *Infinite sinusoidal wave-train.* There is an infinite progressive train of sinusoidal waves, with the wall co-ordinate following the law

$$H = 1 + \phi \sin 2\pi(\xi - \tau), \tag{1}$$

where H is a dimensionless wall co-ordinate, h/a, h the lateral co-ordinate of the wall, ξ a dimensionless transverse co-ordinate, X/λ, X and Y co-ordinates in the laboratory frame, and τ a dimensionless time, ct/λ. The wall itself, however, moves in a purely transverse direction. If the number of waves between the inlet and discharge reservoirs of the pump is finite but integral, the solution for the infinite wave-train remains valid. Presumably most of the important phenomena in peristaltic pumping are not sensitive to the shape of the wave.

(iv) *Fluid properties.* The density and viscosity are assumed constant.

2. Gross pumping performance

2.1. *Theory for plane two-dimensional geometry*

Figure 2 shows the nomenclature used for an infinite sinusoidal wave-train, as observed (upper) in the laboratory frame and (lower) in the wave frame. The transformations between the two frames are

$$x = X - ct, \quad y = Y, \tag{2}$$

and

$$u(x, y) = U(X - ct, Y) - c, \quad v(x, y) = V(X - ct, Y), \tag{3}$$

for velocity components in the laboratory frame, U and V.

Wave frame. It can be shown that, if the tube length is finite but equal to an integral number of wavelengths, and if the pressure difference between the ends of the tube is constant, the flow is steady in the wave frame. For simplicity, we assume that these conditions are met, and we solve the problem in the wave frame. With the assumptions of infinite wavelength and inertia-free flow, the Navier–Stokes equation in the y-direction reduces to

$$\partial p/\partial y = 0, \tag{4}$$

and in the x-direction it becomes

$$\partial p/\partial x = dp/dx = \mu\,\partial^2 u/\partial y^2, \tag{5}$$

for pressure p. Since dp/dx depends upon x but not y, (5) may be integrated twice with respect to y. Using the boundary conditions that

$$\partial u/\partial y = 0 \quad \text{at} \quad y = 0, \qquad u = -c \quad \text{at} \quad y = h,$$

we get a parabolic velocity profile showing the local flow to be of Poiseuille type:

$$\frac{u}{c} = -1 - \frac{a^2}{2\mu c}\frac{dp}{dx}\left[\left(\frac{h}{a}\right)^2 - \left(\frac{y}{a}\right)^2\right]. \tag{6}$$

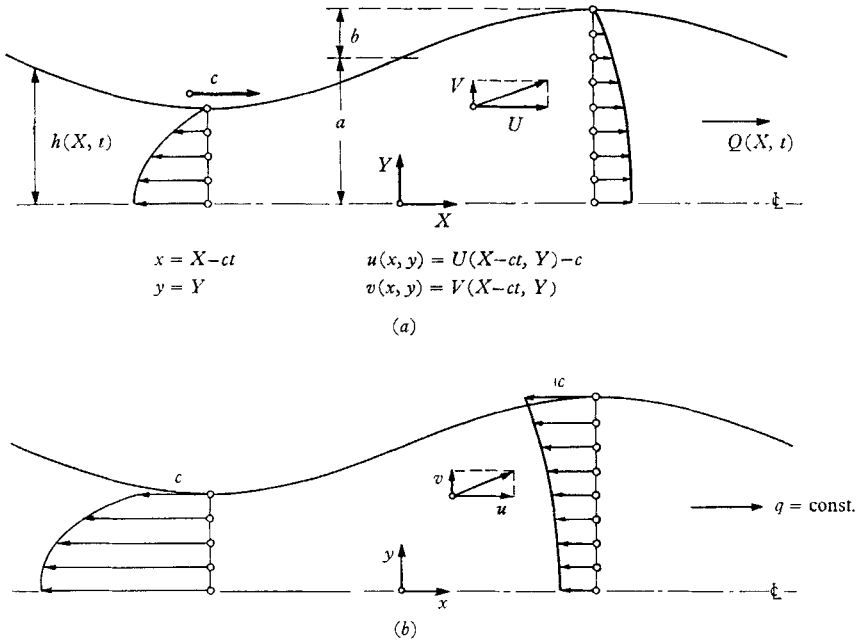

FIGURE 2. Nomenclature for infinite progressive train of sine waves. (*a*) Laboratory frame. (*b*) Wave frame.

The rate of volume flow through each section, q, is a constant, independent of both x and t. It is calculated as

$$q = \int_0^h u\,dy; \tag{7}$$

with (6), this gives

$$\frac{q}{ac} = -\frac{h}{a} - \frac{h^3}{3\mu ca}\frac{dp}{dx}. \tag{8}$$

Laboratory frame. The instantaneous volume flow rate, $Q(X,t)$, is found by integrating

$$Q = \int_0^h U(X, Y, t)\,dY, \tag{9}$$

where Q is instantaneous, local flow observed in the laboratory frame. From (3), $U = u + c$; and the integration leads to

$$Q = q + ch. \tag{10}$$

Considering the peristaltic device as a pump, the quantity of practical interest is the time-mean volume flow at each cross-section, $\bar{Q}$, which measures the mean discharge rate. Using (10), $\bar{Q}$ is calculated by integrating over the period, T:

$$\bar{Q} \equiv \frac{1}{T}\int_0^T Q\,dt = q + \frac{c}{T}\int_0^T h\,dt.$$

The integral, which is to be evaluated with X constant, is found for the sinusoidal wave of (1) to have the value $a\lambda/c$. Hence

$$\bar{Q} = q + ac, \tag{11}$$

which has an obvious physical interpretation.

The pressure rise per wavelength is

$$\Delta p_\lambda \equiv \int_0^\lambda (dp/dx)\,dx. \tag{12}$$

Inserting the value of dp/dx given by (8), substituting h from (1) and q from (11), and introducing dimensionless variables, (12) finally yields

$$\frac{a^2}{\mu c\lambda}\Delta p_\lambda = \frac{3}{2}\frac{\phi^2}{(1-\phi^2)^{\frac{5}{2}}}\left[3 - \frac{2+\phi^2}{\phi}\theta\right]. \tag{13}$$

The denominator of the dimensionless time-mean flow, $\theta \equiv \bar{Q}/bc$, would represent the volume flow rate, if all the material between $y = a-b$ and $y = a+b$ were convected rightwards, like a solid, at speed c. It might be thought of as the 'piston displacement' of the pump. For complete occlusion, $\theta = 1$.

Pressure–flow characteristic. As required by the linear nature of the case $R = 0$, the curve of Δp_λ *vs.* θ is a straight line with negative slope, e.g. figure 7. The relationship between Δp_λ and θ for a fixed value of ϕ may therefore be expressed conveniently by means of the two intercepts: the dimensionless pressure rise $(\Delta p_\lambda)_{\theta=0}$, for zero time-mean flow, and the dimensionless time-mean flow, θ_0, for zero pressure rise. These are given by

$$\frac{a^2}{\mu c\lambda}(\Delta p_\lambda)_{\theta=0} = \frac{9}{2}\frac{\phi^2}{(1-\phi^2)^{\frac{5}{2}}}, \tag{14}$$

$$\theta_0 = \frac{3\phi}{2+\phi^2}. \tag{15}$$

Equations (14) and (15) are plotted in figure 3 over the whole possible range, $\phi = 0$ (no peristalsis) to $\phi = 1$ (complete occlusion).

For $\phi \ll 1$, θ_0 increases linearly with ϕ, while $(\Delta p_\lambda)_{\theta=0}$ increases as ϕ^2. As $\phi \to 1$, $\theta_0 \to 1$, since all the fluid contained in one wavelength must be transported at speed c. Moreover, $(\Delta p_\lambda)_{\theta=0} \to \infty$. Thus the volume flow is independent of the pressure rise, which is the characteristic of a positive-displacement pump. The peristaltic wave serves as a pump in the range where the mean flow is in the direction of the pressure rise, i.e. when $0 \leqslant \theta \leqslant \theta_0$.

Mechanical efficiency. The definition of pumping efficiency consistent with that commonly used for pumping machinery is

$$E \equiv \frac{\bar{Q}\,\Delta p_\lambda}{-\dfrac{1}{T}\displaystyle\int_0^T\int_0^\lambda \left(p + \tau_0\frac{\partial h}{\partial X}\right)\frac{\partial h}{\partial t}\,dX\,dt}. \tag{16}$$

The numerator represents the rate at which useful energy is stored in the fluid, reckoned per wavelength and averaged over the period. The denominator is the rate at which mechanical work is delivered to the wall from outside agencies, again per wavelength and averaged over the period.

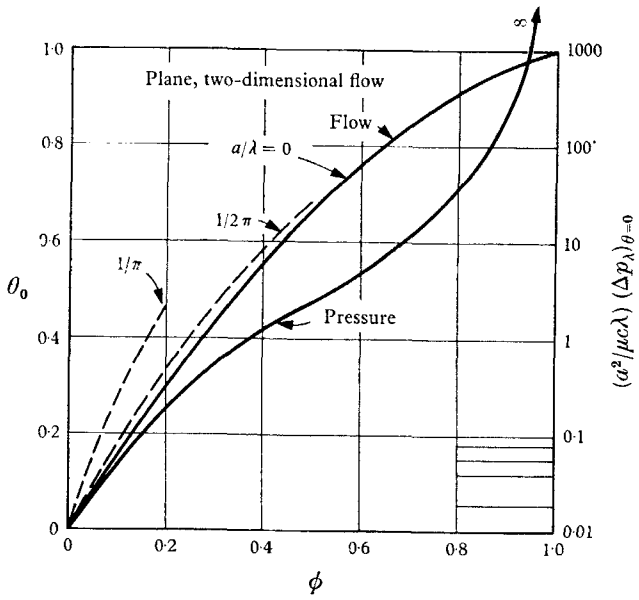

FIGURE 3. Plane case. ——, dimensionless flow θ_0 for zero pressure rise, and dimensionless pressure rise for zero flow, both as functions of amplitude ratio ϕ; — — —, effect of finite wavelength on θ_0 (based on Burns & Parkes 1967).

For $a/\lambda \ll 1$, the contribution of the wall-shear term to the mechanical-work integral is negligible compared with that of the pressure term. Neglecting the former, and using (1), (8) and (13) to evaluate the integral of (16), one obtains

$$E = \frac{(\theta/\theta_0)\,[1-(\theta/\theta_0)]}{\dfrac{(1+2\phi^2)\,(2+\phi^2)}{9\phi^2} - \dfrac{\theta}{\theta_0}}. \tag{17}$$

We might alternatively define an efficiency, E', as

$$E' \equiv 1-(D/\overline{W}),$$

where $\overline{W}$ is the denominator of (16) and D is the rate of viscous dissipation, given by

$$D = \mu \int_0^\lambda \int_0^h \left[2\left(\frac{\partial u}{\partial x}\right)^2 + 2\left(\frac{\partial v}{\partial y}\right)^2 + \left(\frac{\partial u}{\partial y} + \frac{\partial v}{\partial x}\right)^2 \right] dx\,dy.$$

On detailed calculation, E' turns out to be identical with E as given by (17). This shows that the definition used for E properly allocates the mechanical work input into the two components of viscous dissipation and useful energy storage.

The solid curves of figure 4 show E plotted against θ/θ_0 for several values of ϕ.

Where E is important, it is clear that ϕ is large; in that case quite respectable efficiencies are achievable, but over only a relatively narrow range of flows.

At the limit $\phi = 1$, either (i) $\theta = \theta_0$, and Δp_λ is indeterminate, or (ii) $\Delta p_\lambda = \infty$, and $\theta/\theta_0 < 1$, but indeterminate. Of these two possibilities, only the first is of practical interest, since the latter involves infinite velocities through the occluded zone. For $\theta/\theta_0 = 1$, the efficiency is indeterminate, because the viscous dissipation is constant, while the useful mechanical energy stored in the fluid ranges from 0 to ∞. Accordingly, for $\phi = 1$, E ranges from 0, for $\Delta p_\lambda = 0$, to 1, as $\Delta p_\lambda \to \infty$.

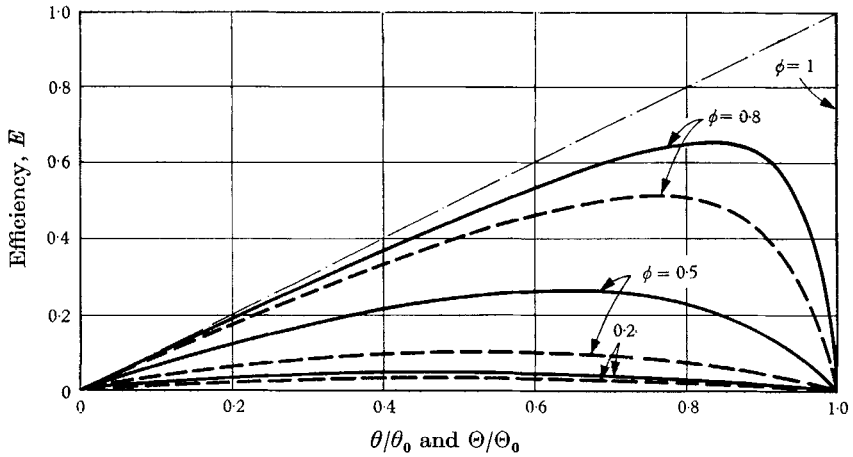

FIGURE 4. Pumping efficiency *vs.* dimensionless flow, θ/θ_0 or Θ/Θ_0. ———, plane, two-dimensional case. — — — —, axisymmetric case.

2.2. *Comparison of results for plane case with other theories*

On figure 3 the dashed curves show the values of θ_0 as computed up to order ϕ^4 in amplitude by Burns & Parkes (1967), for the inertia-free case with arbitrary wavelength. The limiting solution for infinite wavelength (solid curve, $a/\lambda = 0$) is very good up to $a/\lambda = 1/2\pi$. For $a/\lambda = 1/\pi$, the solution for infinite wavelength underestimates the mean flow by about 1/3, at least up to $\phi = 0.2$.

Hanin (1968) gives a formula for θ_0, which takes into account inertial forces, but which is limited to infinite wavelength and is valid up to terms of order ϕ^2 in the amplitude

$$\theta_0 = \tfrac{3}{2}\phi[1 - 0{\cdot}0083R^2].$$

In the inertia-free limit, this reduces to $3\phi/2$, which agrees with (15) when ϕ is small. Moreover, the second term in the square brackets shows that the effect of inertia is less than 1 %, if $R < 1$. Since the typical value of R for the human ureter is about 1 (§ 2.4), it appears that the inertia-free solution is actually quite accurate physiologically, at least when ϕ is not too large.

The two-dimensional solution of § 3.2, when taken to the limit of small ϕ, is identical with that of Fung & Yih, when the latter is taken to the limit of small R.

2.3. *Theory for axisymmetric geometry*

The nomenclature is as in figure 2, except that the transverse co-ordinates are **R** and r rather than Y and y, respectively, while a represents the mean radius. The co-ordinate transformation is $r = \mathbf{R}$.

Wave frame. With the assumptions of infinite wavelength and inertia-free flow, the Navier–Stokes equations have the approximate form

$$\frac{\partial p}{\partial x} = \frac{dp}{dx} = \frac{\mu}{r}\frac{\partial}{\partial r}\left(r\frac{\partial u}{\partial r}\right). \tag{18}$$

Since dp/dx is a function of x only, (18) may be integrated twice with respect to r. Using the boundary conditions that

$$\partial u/\partial r = 0 \quad \text{at} \quad r = 0, \qquad u = -c \quad \text{at} \quad r = h,$$

the parabolic profile of a local Poiseuille flow is obtained once more:

$$\frac{u}{c} = -1 - \frac{a^2}{4\mu c}\frac{dp}{dx}\left[\left(\frac{h}{a}\right)^2 - \left(\frac{r}{a}\right)^2\right]. \tag{19}$$

The constant flow through the tube,

$$q = \int_0^{h^2} \pi u \, d(r^2), \tag{20}$$

is now calculable, with (19) as

$$\frac{q}{\pi a^2 c} = -\left(\frac{h}{a}\right)^2 - \frac{h^4}{8\mu c a^2}\frac{dp}{dx}. \tag{21}$$

Laboratory frame. Noting that

$$Q = \int_0^{h^2} \pi U \, d(\mathbf{R}^2), \tag{22}$$

and using the transformation formulas, we get

$$Q = q + \pi h^2 c. \tag{23}$$

Thus the time-mean volume flow over a period is

$$\bar{Q} \equiv \frac{1}{T}\int_0^T Q \, dt = q + \frac{\pi a^2 c}{T}\int_0^T \left(\frac{h}{a}\right)^2 dt. \tag{24}$$

Integrating for the sinusoidal wall of (1), we get

$$\begin{aligned} \frac{q}{\pi a^2 c} &= \frac{\bar{Q}}{\pi a^2 c} - (1 + \tfrac{1}{2}\phi^2), \\ &= (2\phi - \tfrac{1}{2}\phi^2)\,\Theta - (1 + \tfrac{1}{2}\phi^2), \end{aligned} \tag{25}$$

where

$$\Theta \equiv \frac{\bar{Q}}{\pi a^2 c(2\phi - \frac{1}{2}\phi^2)}, \tag{26}$$

is the dimensionless time-mean volume flow rate. The denominator of this expression is the flow that would be transported if all the material in the tube between

the radii $(a-b)$ and $(a+b)$ were convected rightwards, like a solid body, with speed c. Again, this denominator is a 'piston displacement' for the problem, and $\Theta = 1$ when $\phi = 1$.

Solving for dp/dx from (21), and substituting into (12), we get

$$\Delta p_\lambda = -8\mu c \int_0^\lambda \frac{dx}{h^2} - \frac{8}{\pi}\mu q \int_0^\lambda \frac{dx}{h^4}.$$

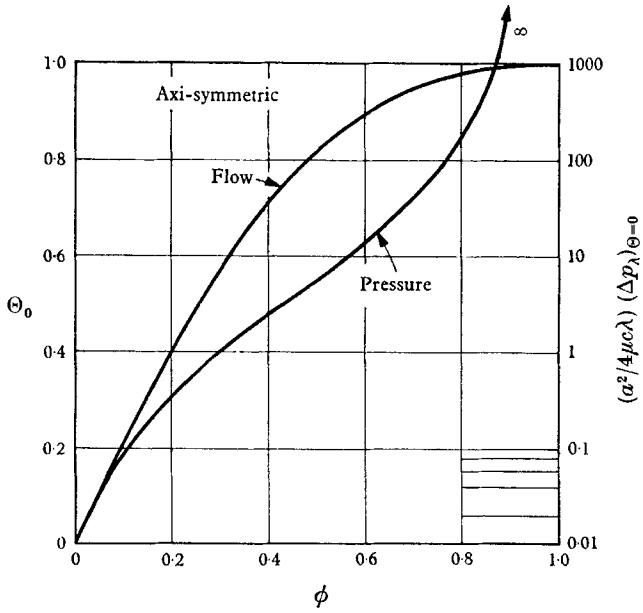

FIGURE 5. Axisymmetric case. Dimensionless flow Θ_0 for zero pressure rise, and dimensionless pressure rise for zero flow, both as functions of amplitude ratio ϕ.

The integrals may be evaluated using (1) for h. Then, substituting q from (25), the results may be brought into the form

$$\frac{a^2}{4\mu c\lambda}\Delta p_\lambda = \frac{8\phi^2(1-\frac{1}{16}\phi^2) - 4\phi(1-\frac{1}{4}\phi)\,(1+\frac{3}{2}\phi^2)\Theta}{(1-\phi^2)^{\frac{7}{2}}}. \tag{27}$$

Pressure–flow characteristic. Since, as in the plane case, the relation between Δp_λ and Θ is linear, we may conveniently characterize the pumping performance in terms of $(\Delta p_\lambda)_{\Theta=0}$ and Θ_0. These are given by

$$\frac{a^2}{4\mu c\lambda}(\Delta p_\lambda)_{\Theta=0} = 8\phi^2\frac{1-\frac{1}{16}\phi^2}{(1-\phi^2)^{\frac{7}{2}}}, \tag{28}$$

$$\Theta_0 = \frac{\phi(4+\phi)}{2+3\phi^2}. \tag{29}$$

They are plotted in figure 5. When $\phi \ll 1$, Θ_0 varies linearly with amplitude, while $(\Delta p_\lambda)_{\Theta=0}$ goes as ϕ^2. As $\phi \to 1$, properly $\Theta_0 \to 1$, and $(\Delta p_\lambda)_{\Theta=0} \to \infty$. The volume flow is constant irrespective of the pressure rise, as in a positive-displacement pump.

Mechanical efficiency. In the axisymmetric case, the denominator of the efficiency expression, (16), is replaced by

$$\overline{W} = -\frac{1}{T}\int_0^T \int_0^\lambda 2\pi hp \frac{\partial h}{\partial t}\, dX\, dt, \tag{30}$$

in which the contribution of τ_0 is negligible for long wavelengths, and has been ignored accordingly. Evaluation of the integral and rearrangement finally lead to

$$E = \frac{(\Theta/\Theta_0)\,[1-(\Theta/\Theta_0)]}{A(\phi)-(\Theta/\Theta_0)}, \tag{31a}$$

where

$$A(\phi) \equiv \frac{4+6\phi^2}{\phi^4(16-\phi^2)^2}\,[4+4(1-\phi^2)^{\frac{7}{2}}+10\phi^2+7\phi^4+\tfrac{3}{2}\phi^6]. \tag{31b}$$

The efficiency, as calculated from (31), is shown in figure 4 by dashed lines, with results similar to those for the plane case.

3. A two-dimensional experiment

A simple quasi-two-dimensional experiment was performed by Latham (1966) in an apparatus shown schematically in figure 6. The test duct was a flattened length of clear, flexible polyvinylchloride tubing with a wall of thickness 0·050 in. This was confined, in a 180° arc, between a flexible steel band and a stationary backplate formed in a semicircle of 16 in. radius, such that the tube became approximately rectangular in shape, height 2·5 in., and mean width about 0·3 in. The ends of the test duct, outside the semicircular arc of flattening, were connected to open vertical reservoirs, in which the fluid could be maintained at constant elevation. The circuit was completed by a control valve, with which the pressure rise between reservoirs was adjusted, and a means for measuring mean volume flow. On the rotating wheel were mounted 32 pairs of adjustable fingers, each of which determined the radial position of a Teflon slider that engaged the flexible band. Since the band itself was constrained against rotation, the sliding fingers imposed on the band a progressive wave of radial displacement. The fingers were adjusted so that there would be an integral number of wavelengths in the active region, approximately sinusoidal in form.

The wave geometry thus established differs in two ways from the theoretical model: (i) the wave is in only one wall, and (ii) the whole duct is curved in a semicircle. These are unimportant differences, however, since the half-width $a = 0{\cdot}15$ in. is small compared with both the wavelength and the radius of the semicircle. Thus the long-wavelength theory remains applicable.

For a fixed wave geometry, the variables that could be adjusted and measured were the wave speed c, the pressure rise Δp_λ, and the viscosity μ; the latter was adjusted and measured by using mixtures of either glycerine and water or corn syrup and water. For each combination a resulting $\bar{Q}$ was measured. Through the choices of c and μ, a very wide range of R was covered, with overlapping ranges of R for different fluids.

Figure 7 shows the experimental results in a case with four wavelengths present and with $\phi = \frac{1}{3}$. The ordinate is the ratio of the measured Δp_λ to the theoretical value given by (14). Bearing in mind (i) that the tube was not exactly two-

dimensional and had curved end walls of variable shape, and (ii) that the wave was only approximately sinusoidal, the agreement between theory and experiment is generally good. For about $R < 0{\cdot}2$, there is no significant effect of Reynolds number within the accuracy of the measurements, as must be true if inertia is unimportant. For about $R > 0{\cdot}2$, however, there is a distinct reduction in pumping performance. The two points for $R = 38$ show a large loss of pumping effectiveness as inertial effects come strongly into play.

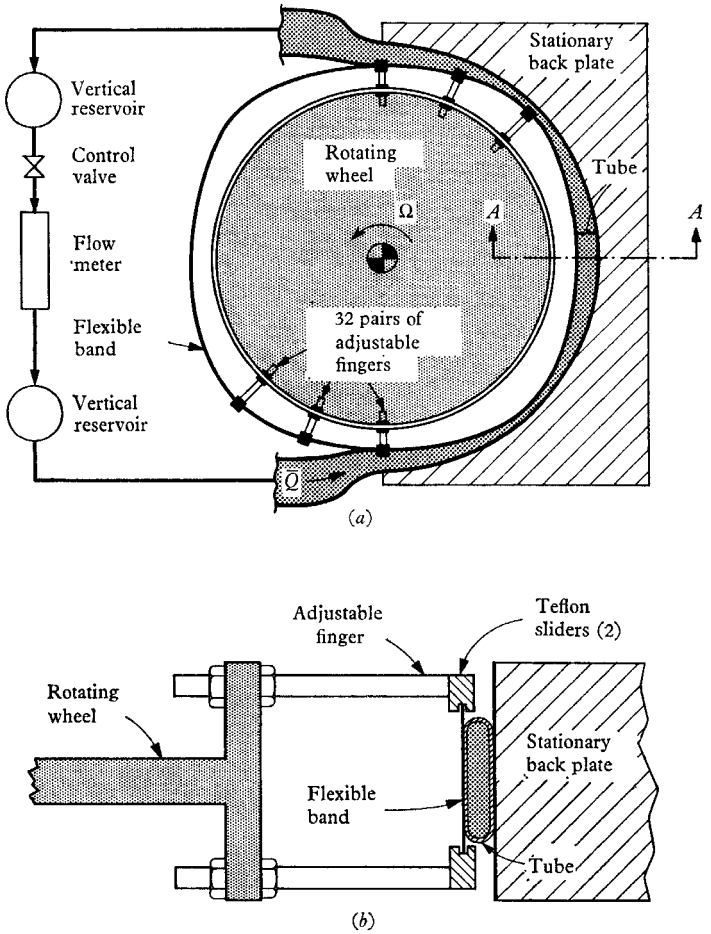

FIGURE 6. Schematic of quasi-two-dimensional experiment (Latham 1966): (*a*) plan view, (*b*) section A–A.

4. Details of fluid motion (plane case)

4.1. *Velocity distributions and the wave frame stream function*

Longitudinal velocity. Using the transformation of (3), and applying (1), (8) and (11) to (6), the longitudinal velocity distribution in the laboratory frame may be expressed as

$$\frac{U}{c} = \frac{\frac{3}{2}\phi}{1+\phi\sin 2\pi(\xi-\tau)}\left[\theta+\sin 2\pi(\xi-\tau)\right]\left[1-\left(\frac{\eta}{H}\right)^2\right]. \tag{32}$$

Since U/c varies parabolically over each cross-section, from zero at the wall to a maximum (or minimum) at the axis of symmetry, we may visualize the longitudinal velocity distribution merely by examining U/c at the axis, $\eta = 0$. From (32) it may be shown that $(U/c)_{\eta=0}$ is a maximum when $\xi = \frac{1}{4}$, i.e. at the widest part of the channel, and that it is a minimum when $\xi = \frac{3}{4}$, i.e. at the narrowest part of the channel. The values are respectively

$$(U/c)_{\eta=0,\,\max} = \tfrac{3}{2}(1+\theta)\,\phi/(1+\phi), \tag{33a}$$

$$(U/c)_{\eta=0,\,\min} = -\tfrac{3}{2}(1-\theta)\,\phi/(1-\phi). \tag{33b}$$

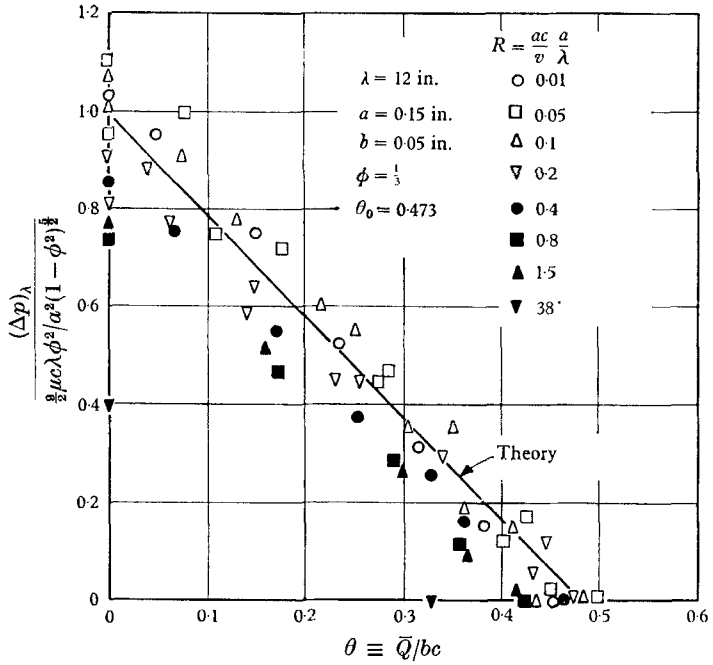

FIGURE 7. Experimental results for the plane case (Latham 1966). The abscissa is the dimensionless time-mean flow. The ordinate is the ratio of the measured pressure rise to the theoretical rise for zero flow.

These are plotted in figure 8 for the two limits of the range of θ in which the peristaltic wave acts as a pump. In this range, the maximum value of U/c is always positive, while the minimum is always negative. The latter may become very large at large ϕ.

A sidelight on these results for the infinite sinusoidal wave-train is that they agree with the very simple notion of peristaltic pumping described in § 2.2 and figure 1.

Transverse velocity. From the continuity equation, we may calculate the transverse velocity from the integral

$$V = -\int_0^Y \frac{\partial U}{\partial X}\,dY,$$

which, with (32), leads to

$$\frac{V}{c} = -3\pi \frac{b}{\lambda}\left[\frac{1-\phi\theta}{H}\frac{\eta}{H} + \left(\frac{2}{3} - \frac{1-\phi\theta}{H}\right)\left(\frac{\eta}{H}\right)^3\right]\cos 2\pi(\xi-\tau). \tag{34}$$

Stream function in the wave frame. In the laboratory frame the flow is unsteady, and the particle path lines, e.g. figure 9, are very different from the streamlines, e.g. Burns & Parkes (1967, figure 4). The flow in the wave frame, on the other

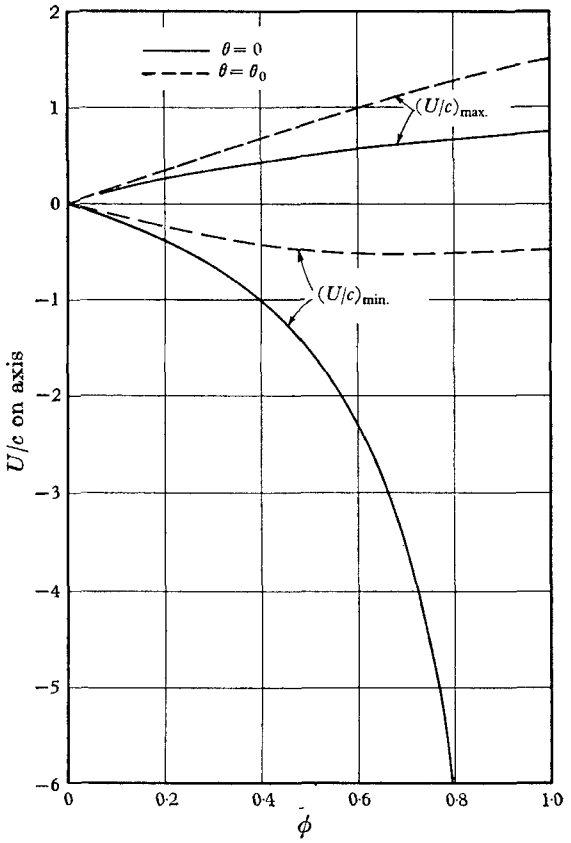

FIGURE 8. Plane case. Maximum and minimum values of U/c on the axis, for the two limits $\theta = 0$ and $\theta = \theta_0$.

hand, is steady; hence the path lines, streamlines, and streaklines all coincide. They are usually similar to the wall shape, but with lesser amplitude as the axis is approached, with the exception of certain cases where a region of closed streamlines is present, e.g. figure 11.

The stream function in the wave frame is later put to important use as a quantitative marker for identifying material fluid particles in the laboratory frame. Defining it as

$$d\psi = u\,dy - v\,dx,$$

and using (8), (32) and (34) for the velocity distributions, integration leads to

$$\chi \equiv \frac{\psi}{ca} = \left[\frac{H-(1-\phi\theta)}{2}\right]\left[3\frac{\eta}{H}-\left(\frac{\eta}{H}\right)^3\right]-\eta, \tag{35}$$

where ψ has been set equal to zero on the axis. Its value at the wall is

$$\chi_w = \phi\theta - 1. \tag{36}$$

In appendix B, (35) is obtained alternatively by a solution of the zeroth-order approximation to the Navier–Stokes equations expressed in terms of the stream function.

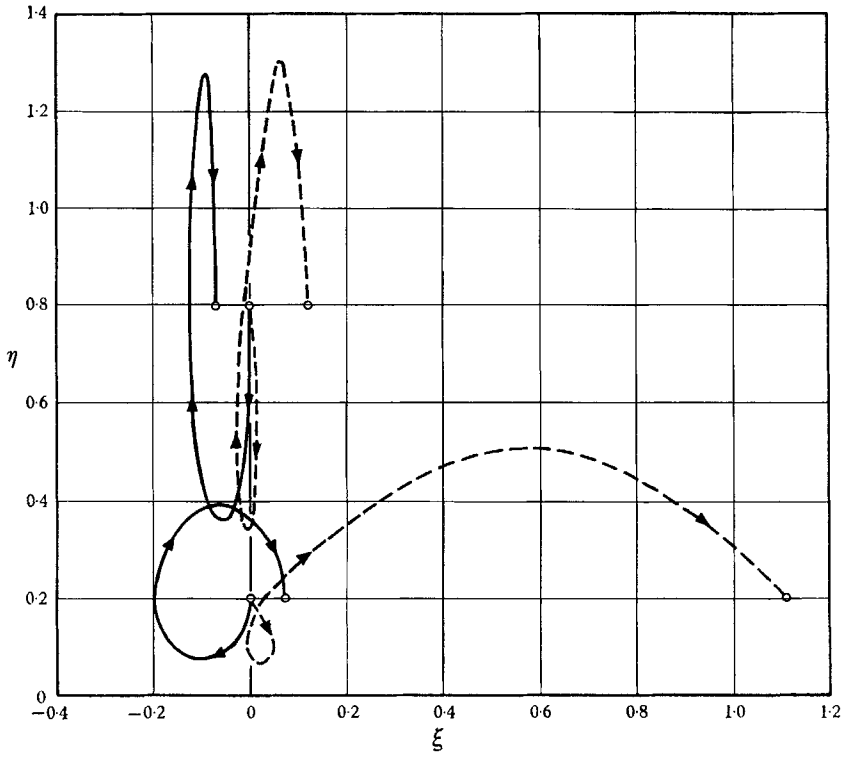

FIGURE 9. Samples of particle trajectories for the plane case, with $\phi = \frac{1}{2}$: two-dimensional; sine wave; particle orbits for $\eta_0 = 0{\cdot}2$, $\eta_0 = 0{\cdot}8$ at $\tau = 0$ and $\xi = 0$. ———, $\theta/\theta_0 = 0$; — — — —, $\theta/\theta_0 = 1$.

4.2. *Mean displacement profiles for material particles*

One manifestation of 'ureteral reflux' is that bacteria sometimes travel from the bladder to the kidneys, against the mean urine flow. This happens in a matter of hours, much too rapidly to be explained by molecular diffusion, even when it is enhanced by bacterial self-propulsion. The phenomenon seems explicable through calculations of the net displacement histories of parcels of fluid of fixed identity. The trajectories of fluid parcels may clearly be of importance also in the functioning of the gastro-intestinal tract, where chemical reactions

between the contents and materials at the walls will be affected by convective transport.

From (32) and figure 8, it is evident that, at a fixed cross-section, the fluid moves alternately with and against the wave at different phases of the wave's passage. This behaviour might influence functioning of the ureter and gastro-intestinal tract through a coupling between longitudinal convective transport and transverse diffusive transport, leading to an augmentation of net longitudinal diffusion.

However, a more direct and powerful fluid mechanism for redistributing materials is potentially present in peristaltic pumping. It might be thought that the net displacement of the fluid in the laboratory frame could be related to the time-mean longitudinal velocity at each point (the time-mean transverse velocity is zero). But in fact the time-mean longitudinal velocity tells very little about where the fluid goes; indeed, it is quite possible for the time-mean velocity at a fixed point to be negative, while the net displacement of a fluid particle, per cycle, is positive. In order to arrive at a meaningful result, we must calculate the trajectories of material fluid particles by integrating the simultaneous equations

$$d\xi/d\tau = U/c, \quad d\eta/d\tau = (V/c)\,(\lambda/a), \tag{37}$$

where U/c and V/c are each functions of ξ, η and τ as given by (32) and (34).

By observing that the particle trajectories in the wave frame are periodic, it can be shown that the particle trajectories in the laboratory frame are repetitive, with a characteristic period $\Delta\tau^*$. This latter is defined as the time interval between two successive instants at which the particle occupies the same position relative to the wave.

Particles on the axis. The integration may be performed analytically for particles on the axis, $\eta = 0$,with results that are instructive. In a certain range of ϕ and θ/θ_0, a material particle on the axis executes periodic displacements, with both positive and negative contributions to the net displacement. Let the period of the particle trajectory be $\Delta\tau^*$, and the corresponding net displacement be $\Delta\xi^*$; then, within this range defined by $\theta/\theta_0 \leqslant (2-\phi)\,(2+\phi^2)/9\phi^2$, one can show that

$$\Delta\xi^* = 3\left[\frac{1-\phi\theta}{\sqrt{\left[(1-\frac{3}{2}\phi\theta)^2-\left(\frac{\phi}{2}\right)^2\right]}}-1\right], \tag{38}$$

$$\Delta\tau^* = 1+\Delta\xi^*. \tag{39}$$

Surprisingly, the period $\Delta\tau^*$ of the particle trajectory is not unity (the period of the wave). The wave is progressive, and there is a net displacement $\Delta\xi^*$; thus the particle must travel for a time either slightly greater or slightly less than one wave period, in order to find itself again in the same position relative to the wave. The mean speed of displacement of the particle, averaged over the particle period, is

$$S \equiv \Delta\xi^*/\Delta\tau^*. \tag{40}$$

In the pumping range, $0 \leqslant \theta \leqslant \theta_0$, S is positive for all values of ϕ. It is surprising that this should be so. When $\theta = 0$, for instance, particles on the axis

make net headway in the direction of the wave, even though $\bar{Q} = 0$. But such can only be the case if particles at some distance from the axis make net headway in the direction opposite to the wave. The magnitudes of these displacements are by no means negligible. When $\theta = 0$ and $\phi = 0{\cdot}8$, for instance, $S \approx 0{\cdot}2$; this means that in one particle period, in this case about 1·2 wave periods, a fluid parcel on the axis moves about 20 % of a wavelength in the direction of the wave.

Particles not on the axis. Equations (37) are in general not integrable in terms of elementary functions, and numerical integrations are therefore necessary.

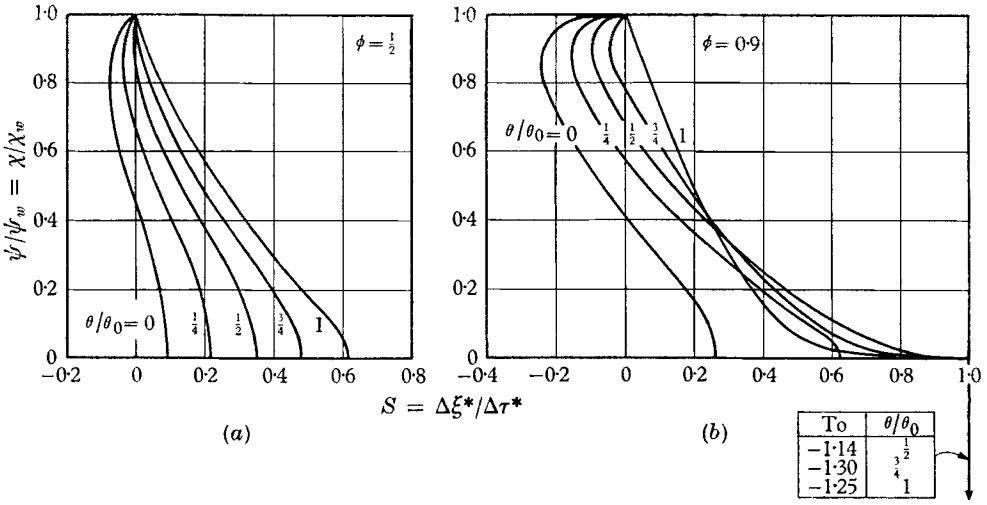

FIGURE 10. Curves of mean speed of advance, S, for material particles, plotted against the value of the wave frame stream function identifying the particle. (*a*) For $\phi = \frac{1}{2}$, (*b*) for $\phi = 0{\cdot}9$.

Figure 9 shows the results for a typical case, with $\phi = \frac{1}{2}$, and for $\theta/\theta_0 = 0$ and $\theta/\theta_0 = 1$. Two starting positions of the particle are shown, one near the axis ($\eta_0 = 0{\cdot}2$ at $\xi = 0, \tau = 0$), the other near the wall ($\eta_0 = 0{\cdot}8$ at $\xi = 0, \tau = 0$). Each trajectory is shown for one period of the particle motion, which is then repetitive. For $\theta = 0$, the particle near the axis experiences in one period a net positive displacement of about 0·1 wavelength, and for $\theta = \theta_0$ about 1·1 wavelengths. The particle near the wall experiences a net negative displacement of about 0·1 wavelength for $\theta = 0$, and a net positive displacement also of about 0·1 wavelength for $\theta = \theta_0$.

Reflux phenomenon. If the profile of mean speed of advance S were displayed as a function of lateral position η, its shape would depend upon the longitudinal position ξ. A more meaningful plot, free of this ambiguity, is that of figure 10, in which the mean speed S of the material particle is plotted against that value of the dimensionless stream function χ/χ_w which identifies the material particles on the wave frame streamline χ.

In figure 10(*a*) typical profiles of S *vs.* χ/χ_w are shown for $\phi = \frac{1}{2}$ and for several values of θ/θ_0 between 0 and 1. For values of θ/θ_0 up to about $\frac{3}{4}$, the net forward flow is seen to be the difference between a forward flow near the axis and a reverse

flow near the wall. This reflux phenomenon clearly represents a possible explanation for the transport of bacteria in the ureter from the bladder to the kidneys in a direction opposite to that of the mean discharge.

Trapping phenomenon. Figure 10(*b*) shows the profiles of S *vs.* χ/χ_w for a larger amplitude ratio, $\phi = 0{\cdot}9$. The results are similar to those of figure 10(*a*), except for an additional feature. There exist streamlines with negative values of χ/χ_w; on all such streamlines, $S = 1$. The associated fluid has a mean speed of advance exactly equal to the wave speed. This fluid is 'trapped' in that it moves, at least in the mean, with the wave itself.

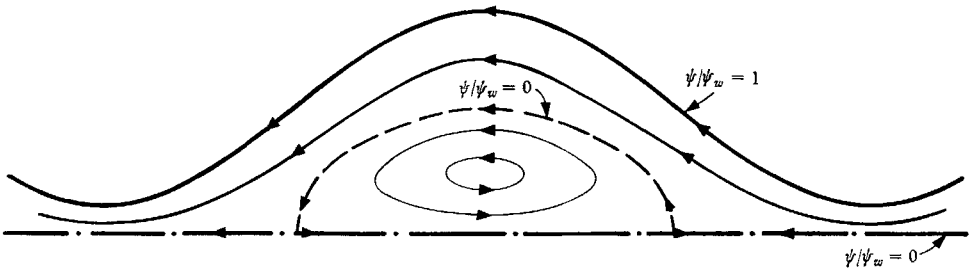

FIGURE 11. Streamlines in wave frame for a combination of amplitude and flow such that a trapped bolus exists in the laboratory frame.

To elucidate this, figure 11 shows schematically the streamlines in the wave frame, as determined by (35), for combinations of ϕ and θ such that trapping occurs. The centre streamline splits, and there is a region of recirculating, closed streamlines. This region comprises a bolus of fluid which, in the laboratory frame, is trapped with the wave in the sense that it advances as a whole with the speed c. Although there is an internal circulation within the bolus, all fluid particles in the trapped bolus move with a mean advance speed equal to c.

4.3. *Quantity of reflux flow*

In order to get a measure of the rate of reflux of material as a proportion of the net flow, we use ψ as an indicator of material particles, and proceed to calculate the time-mean flow in the lab frame between the axis and a particular value of ψ. The instantaneous flow Q_ψ of all the material between the axis and the co-ordinate ψ is

$$Q_\psi = \int_0^{Y(\psi, X, t)} U(X, Y, t)\, dY. \tag{41}$$

Using the transformations between the two frames and the definition of the wave frame stream function ψ, and taking the time-mean over the period T, we get

$$\bar{Q}_\psi = \psi + \frac{c}{T}\int_0^T y(\psi, X, t)\, dt. \tag{42}$$

Since the integral is to be evaluated at constant X, we may substitute $dt = (1/c)\, dx$ and perform the integral in the wave frame. Normalizing with respect to ca, and introducing the dimensionless variables η and ξ, we obtain

$$\frac{\bar{Q}_\psi}{ca} = \chi + \int_0^1 \eta(\chi, \xi)\, d\xi. \tag{43}$$

This has the physical interpretation that the time-mean flow in the laboratory frame of the material between the co-ordinates $\psi = 0$ and $\psi = \psi$ is the sum of (a) the steady flow as seen in the wave frame between these two streamlines and (b) the average flow in one period, if all the material in one wavelength between the axis and the wave frame streamline were transported rightwards as a solid block with the speed c.

The integrand of (43) is found by solving (35), a cubic, for η as a function of ξ. Except for special limiting cases, the integral has to be determined by numerical quadrature.

Significance of curves of $\bar{Q}_\psi$ vs. ψ. Depending upon the values of ϕ and θ, the curves of $\bar{Q}_\psi$ *vs.* ψ are of four different types. These are shown schematically in figure 12, in which both co-ordinates are normalized in terms of their respective values at the wall. Unity on the vertical scale represents the time-mean flow for the whole passage. Curve I represents a case with neither reflux nor trapping. Curve II represents a case without reflux. However, the part of the curve between '0' and 'a' represents a trapped bolus, which moves with the wave speed. The height of the intersection 'a' is the bolus flow expressed as a fraction of the net flow. Curve III signifies reflux without trapping. Between the origin and point 'b', the material advances in the direction of the wave; between 'b' and the upper terminus of the curve, the material moves in a direction opposite to that of the wave. The distance '$\mathscr{R}$' represents the ratio of reflux flow as a fraction of the net flow. Curve IV represents a situation with both trapping and reflux.

Reflux limit. The combinations of ϕ and θ for which reflux occurs may be found analytically by a perturbation expansion about the point (1, 1) in figure 12. Considering wave frame streamlines very close to the wall, we introduce the small parameter

$$\epsilon \equiv \chi - \chi_w = \chi + (1 - \phi\theta). \tag{44}$$

Then we suppose that the equation of a streamline near the wall, which must of course have nearly the shape of the wall, may be expressed as

$$\eta(\xi;\, \phi, \theta, \epsilon) = H + a_1(\xi;\, \phi, \theta)\,\epsilon + a_2(\xi;\, \phi, \theta)\,\epsilon^2 + \ldots.$$

Introducing this and (44) into (35), and determining the coefficients a_1, a_2, ..., we get

$$\eta = H - \epsilon - \frac{3}{2}\frac{\epsilon^2}{H}\left(\frac{\phi\theta - 1}{H} + 1\right) + \ldots. \tag{45}$$

On applying this to the integral of (43), the result is

$$\frac{\bar{Q}_\psi}{ac} = \phi\theta - \frac{3}{2}\frac{\epsilon^2(\phi\theta - \phi^2)}{(1-\phi^2)^{\frac{5}{2}}} + \ldots. \tag{46}$$

This result shows that the curves of figure 12 all have zero slope at (1, 1). The condition that $\bar{Q}_\psi/\bar{Q}_w$ rise above unity, i.e. that reflux occur, is simply $\phi\theta < \phi^2$, or

$$\frac{\theta}{\theta_0} < \frac{2 + \phi^2}{3}. \tag{47}$$

Solution for small amplitudes. The reflux fraction $\mathscr{R}$ may be determined in closed form for small values of ϕ. Restricting the calculations to the pumping

range, (15) shows that $\phi\theta$ is of order ϕ^2 or less. Further, $(H-1)$ is of order ϕ. Examination of (35) then suggests that the equation of the streamlines be expanded in a power series in the small parameter ϕ:

$$\eta(\xi;\phi,\theta,\chi) = -\chi[1+b_1(\xi;\theta,\chi)\phi+b_2(\xi;\theta,\chi)\phi^2+\ldots]. \tag{48}$$

Substituting this into (35), and determining the coefficients b_1, b_2, ..., we get

$$\eta = -\chi\{1+\tfrac{3}{2}(1-\tfrac{1}{3}\chi^2)(\theta+\sin 2\pi\xi)\phi+\tfrac{3}{4}[(\chi^2-1)^2\sin^2 2\pi\xi]\phi^2+\ldots\}. \tag{49}$$

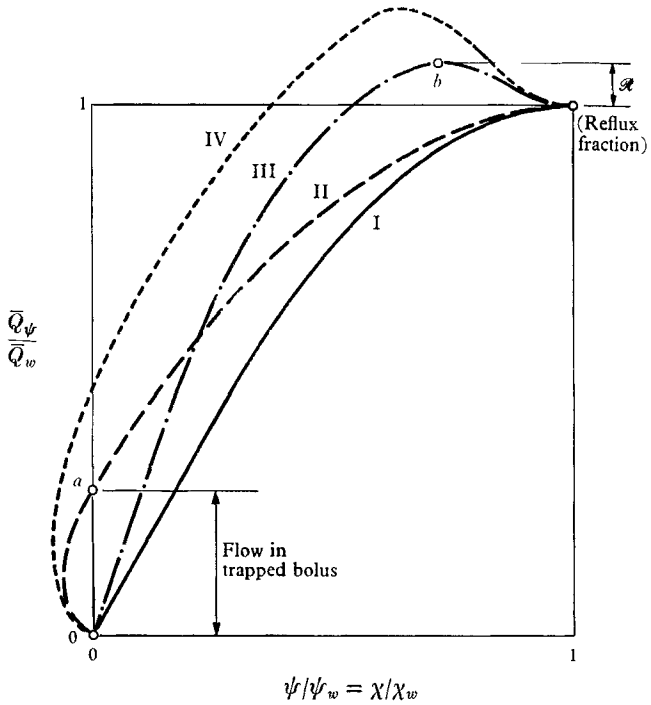

FIGURE 12. Qualitative curves of the dimensionless time-mean flow $\bar{Q}_\psi$ between the axis, and the corresponding value of the wave frame stream function ψ, plotted against the dimensionless value of ψ.

When this is used to evaluate the integral of (43), the result is

$$\frac{\bar{Q}_\psi}{ca} = -\tfrac{3}{2}\chi\phi^2\left[\frac{(\chi^2-1)^2}{4}+\frac{\theta}{\phi}\left(1-\frac{\chi^2}{3}\right)\right]. \tag{50}$$

Setting $(d/d\chi)(\bar{Q}_\psi/ca) = 0$, a maximum for $\bar{Q}_\psi$ is found from (50) to occur at $\chi^2 = \frac{1}{5}[1+(4\theta/\phi)]$, and the fraction of reflux may then be calculated as

$$\mathscr{R} = \frac{(\bar{Q}_\psi/ca)_{\max}}{\phi\theta}-1 = \frac{\left(1+\dfrac{12}{2+\phi^2}\dfrac{\theta}{\theta_0}\right)^{\frac{3}{2}}}{\dfrac{25\sqrt{5}}{2+\phi^2}\dfrac{\theta}{\theta_0}}\left(2-\frac{\theta/\theta_0}{2+\phi^2}\right)-1. \tag{51}$$

4.4. *The trapping limit*

Proceeding from (35), it may be shown that $\chi = 0$ not only on the axis but also on the curve defined by

$$\eta^2 = H^2 \frac{3\phi\theta - 2 + \phi \sin 2\pi\xi}{\phi(\theta + \sin 2\pi\xi)}. \tag{52}$$

Analysis of this equation shows that the curve is real, cuts the centreline, and lies within the tube if

$$\frac{(2-\phi)(2+\phi^2)}{9\phi^2} < \frac{\theta}{\theta_0} < \frac{(2+\phi)(2+\phi^2)}{9\phi^2}. \tag{53}$$

These are the conditions for which there will exist closed streamlines forming a trapped bolus moving at the speed of the wave.

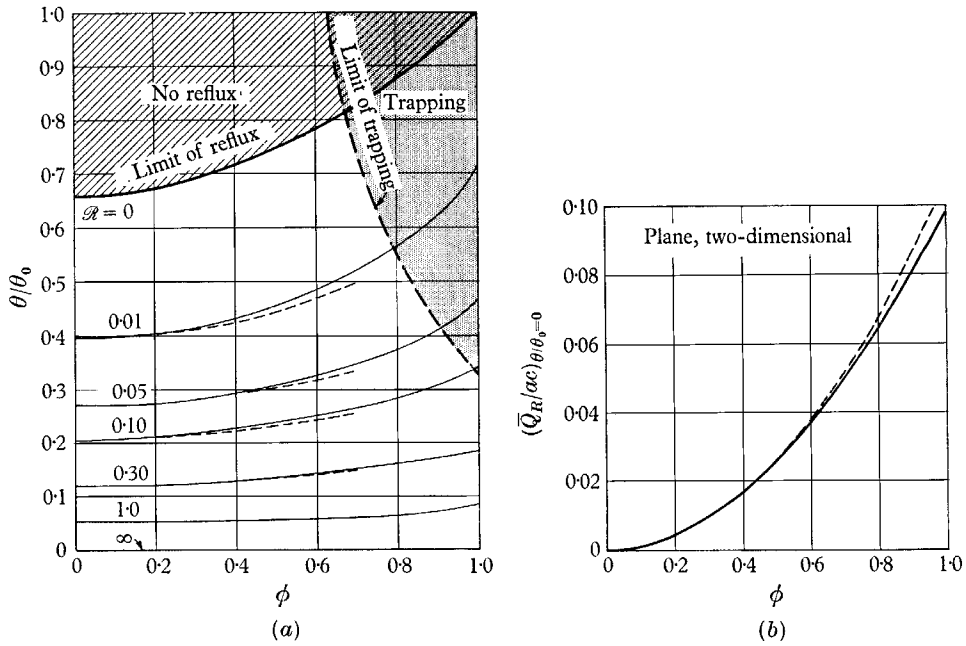

FIGURE 13. Summary charts for plane case: (*a*) trapping limit, reflux limit, and curves of constant reflux fraction $\mathscr{R}$; (*b*) dimensionless reflux flow for the limit $\theta/\theta_0 = 0$. — — —, expansion solution up to terms in ϕ^2.

4.5. *A graphical summary*

Figure 13(*a*) expresses concisely the results of practical interest for the range $0 < \theta < \theta_0$. Using ϕ and θ/θ_0 as co-ordinates, the régimes of reflux and of trapping are shown, as well as curves of constant fraction of reflux. For $\phi \geqslant 0{\cdot}1$, $\mathscr{R}$ was found through numerical integration of (43), using the interpretation of figure 12. The dashed curves for constant $\mathscr{R}$ were calculated from (51), representing the expansion solution up to terms of order ϕ^2; the agreement is quite good up to $\phi = 0{\cdot}7$. The limit of reflux was calculated from (47). The limit of trapping was determined from the lower limit of (53); the upper limit of (53) applies only to $\theta > \theta_0$, outside the pumping range. From the limit curve for reflux in figure 13(*a*),

it appears that reflux may be quite common in the pumping range, since it occurs for values of θ/θ_0 up to about 0·7, with small wave amplitudes, and for values of θ/θ_0 up to nearly unity, with large wave amplitudes.

The reflux fraction $\mathscr{R}$ is quite small when θ/θ_0 exceeds about half the limit value for reflux. When θ/θ_0 is small, on the other hand, say of the order of 0·05 or less, $\mathscr{R}$ is 100 % or more. Indeed, as $\theta/\theta_0 \to 0$, $\mathscr{R} \to \infty$, because the net flow goes to zero, while the reflux flow remains finite. Therefore it is useful to know the absolute magnitude of the reflux flow $\bar{Q}_R$ for small values of θ/θ_0. This is plotted in figure 13(*b*) as a function of ϕ for the limiting case $\theta/\theta_0 = 0$. The dashed curve, representing the expansion solution up to terms of order ϕ^2, is in surprising agreement even up to $\phi = 1$. Using the value of $(\bar{Q}_R/ac)_{\theta=0}$ given by figure 13(*b*), the reflux fraction for very small values of θ/θ_0 may be approximated as

$$(\mathscr{R}_{\theta/\theta_0 \to 0})\,\frac{\theta}{\theta_0} \cong \frac{2+\phi^2}{3\phi^2}\left(\frac{\bar{Q}_R}{ac}\right)_{\theta/\theta_0=0}. \tag{54}$$

4.6. *Experimental verification of reflux*

A preliminary experiment to test the theoretical prediction of reflux was performed in the apparatus of figure 6. Dyed fluid was injected near the wall with $\theta = 0$. The dyed fluid was seen to move alternately with and against the wave, but with a new displacement per period opposite to that of the wave. The trajectory was of the same character as the solid curve starting at $\eta_0 = 0{\cdot}8$ in figure 9.

5. Details of fluid motion (axisymmetric case)

The concepts and procedures for the axisymmetric case are identical with those for the plane case, although the details of calculation are more extensive. We summarize here only the principal results.

5.1. *Velocity distributions and the wave frame stream function*

$$\frac{U}{c} = 2\left(1+\frac{1}{H^2}\frac{q}{\pi a^2 c}\right)\left(1-\frac{\eta^2}{H^2}\right), \tag{55}$$

$$\frac{V}{c} = 2\pi\frac{b}{\lambda}\left[2\frac{q}{\pi a^2 c}\frac{\eta}{H^3}-\left(1+\frac{2}{H^2}\frac{q}{\pi a^2 c}\right)\frac{\eta^3}{H^3}\right]\cos 2\pi(\xi-\tau), \tag{56}$$

where $q/\pi a^2 c$ is given by (25). The maximum and minimum values of U/c on the axis are shown in figure 14 for $\Theta = 0$ and for $\Theta = \Theta_0$.

Introducing Stokes's stream function in the wave frame, defined by

$$d\psi = 2\pi r u\,dr - 2\pi r v\,dx,$$

the result is

$$\frac{\psi}{\pi a^2 c} = \eta^2 - \frac{\eta^4}{H^2} + \frac{q}{\pi a^2 c}\left(2\frac{\eta^2}{H^2}-\frac{\eta^4}{H^4}\right), \tag{57a}$$

$$\psi_w/\pi a^2 c = q/\pi a^2 c. \tag{57b}$$

5.2. *Trapping limit*

A trapped bolus moves with the wave when

$$\frac{(1-2\phi)(2+3\phi^2)}{(16-\phi^2)\phi^2} < \frac{\Theta}{\Theta_0} < \frac{(1-2\phi)(2+3\phi^2)}{(16-\phi^2)\phi^2}. \tag{58}$$

The lower limit is shown in figure 15, while the upper limit occurs only for $\Theta > \Theta_0$, i.e. outside the pumping range.

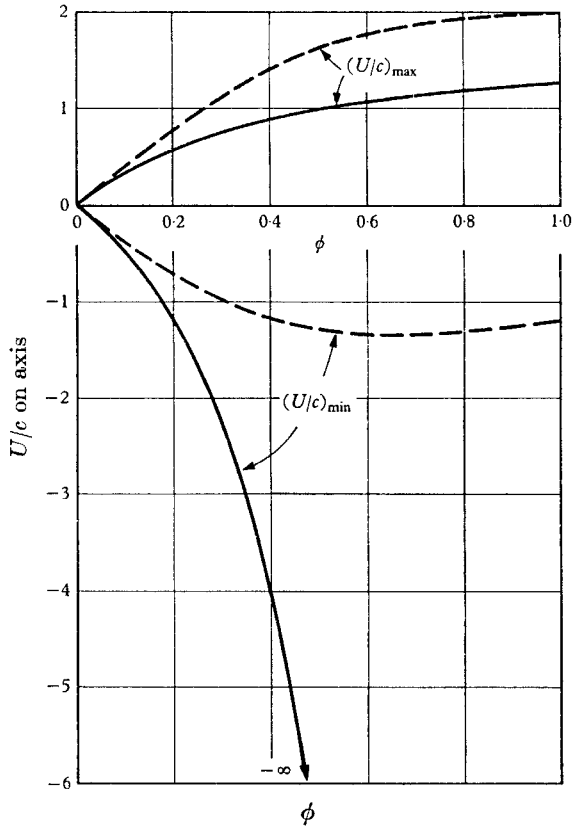

FIGURE 14. Axisymmetric case. Maximum and minimum values of U/c on the axis, for the two limits $\Theta = 0$ and $\Theta = \Theta_0$. ——, $\Theta = 0$; — — —, $\Theta = \Theta_0$.

5.3. *Reflux limit*

A perturbation calculation such as that used in the plane case leads to the result that reflux occurs whenever $\Theta/\Theta_0 < 1$, but not for higher values. That is, reflux occurs over the entire pumping range; evidently it is the rule rather than the exception.

5.4. *Reflux fraction for small amplitude*

Again using a power-series expansion in ϕ, as for the plane case, the reflux fraction as $\phi \to 0$ may be calculated as

$$\mathscr{R}_{\phi=0} = \frac{(1+2[\Theta/\Theta_0])^2}{27\Theta/\Theta_0}\left(4-\frac{\Theta}{\Theta_0}\right) - 1. \tag{59}$$

6.5. *A graphical summary*

Using ϕ as abscissa and Θ/Θ_0 as ordinate, figure 15(*a*) shows the trapping limit, the reflux limit, and curves of constant reflux fraction. As in the plane case, the latter required numerical integration. Except when $\Theta/\Theta_0 > \frac{1}{2}$ or so, $\mathscr{R}$ is quite large. As $\Theta/\Theta_0 \to 0$, $\mathscr{R} \to \infty$. The absolute value of reflux flow is accordingly shown in figure 15(*b*) at this limit.

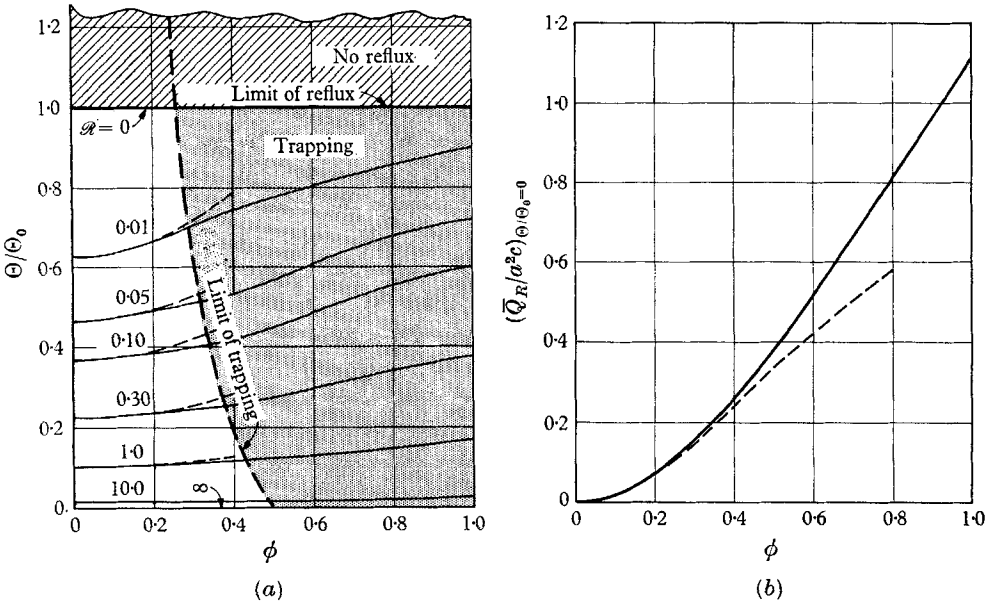

FIGURE 15. Summary charts for axisymmetric case: (*a*) trapping limit, reflux limit, and curves of constant reflux fraction $\mathscr{R}$ (the domain of trapping is shown only for $\Theta/\Theta_0 \leqslant 1$); (*b*) dimensionless reflux flow for the limit $\Theta/\Theta_0 = 0$. — — — —, expansion solution up to terms in ϕ^2.

The research was supported in part by the Office of Naval Research, Contract N 00014-67-A-0204-0008, NR 062-400/1-11-67. E. Eckstein assisted with the visualization of the reflux flow. D. L. McGraith helped with computer programming. Computation services were supplied by the M.I.T. Computation Centre.

Appendix A

Of the several different Reynolds numbers, R, that might be defined, it is not immediately obvious which best serves as a measure of the relative ratio of inertial to viscous forces. For flows in which inertial effects are relatively weak (the case where one seeks the limits of the inertia-free solution), the appropriate R may be found by calculating *a posteriori* the inertial and viscous terms of the inertia-free solution, treating the latter as the zeroth-order solution pertaining to $R = 0$.

In the two-dimensional case,

$$R \equiv \left(u\frac{\partial u}{\partial x} + v\frac{\partial u}{\partial y}\right) \Big/ \nu\frac{\partial^2 u}{\partial y^2}$$

is readily found from (3), (32) and (34) to have the following value on the axis:

$$R = \frac{\pi}{2}\frac{ac}{\nu}\frac{a}{\lambda}\frac{(\phi\theta - 1)(3\phi\theta - 2 + \phi\sin 2\pi\xi)\cos 2\pi\xi}{\theta + \sin 2\pi\xi}.$$

Since both θ and $\phi\theta$ lie in the range between zero and unity, the R appropriately characterizing flows with small inertial effects is $R = (ac/\nu)(a/\lambda)$.
The same result can be shown to be correct in the axisymmetric case.

Appendix B

The full Navier–Stokes equations for the plane case, expressed in wave frame co-ordinates, and in terms of the wave frame stream function, are reducible to

$$\psi_y \nabla^2\psi_x - \psi_x \nabla^2\psi_y = \nu\nabla^2\nabla^2\psi: \tag{B 1}$$

see Schlichting (1968, p. 69). All the physical quantities of (B 1) can be brought approximately to the scale of unity through the introduction of the following dimensionless variables:

$$\xi \equiv x/\lambda, \quad \eta \equiv y/a, \quad \chi \equiv \psi/ac,$$

$$\beta \equiv a/\lambda, \quad R \equiv (ac/\nu)\beta.$$

Expressed in these variables, (B 1) becomes

$$R[\chi_\eta(\chi_{\eta\eta\xi} + \beta^2\chi_{\xi\xi\xi}) - \chi_\xi(\chi_{\eta\eta\eta} + \beta^2\chi_{\eta\xi\xi})] = \chi_{\eta\eta\eta\eta} + 2\beta^2\chi_{\eta\eta\xi\xi} + \beta^4\chi_{\xi\xi\xi\xi}. \tag{B 2}$$

Thus the two parameters β and R govern the problem: the solution may be expressed as power-series expansions in them, if they are small compared with unity. For the zeroth-order term of the series, (B 2) yields

$$\chi_{\eta\eta\eta\eta} = 0. \tag{B 3}$$

Although this corresponds to $\beta \ll 1$ and $R \ll 1$, (B 3) remains valid even for quite high values of $R = ac/\nu$, provided that the wave-number β is sufficiently small. Now, the boundary conditions for (B 3) were:

$$\chi = 0, \quad \chi_{\eta\eta} = 0 \quad \text{at} \quad \eta = 0;$$

$$\chi_\eta = -1, \quad \chi = q/ac \quad \text{at} \quad \eta = H.$$

Using these, the solution obtained is precisely that given by (35).

A similar analysis may be made for the axisymmetric case.

REFERENCES

BOYARSKY, S. 1964 Surgical physiology of the renal pelvis and ureter. *Monogr. Surg. Sci.* **1**, 173–213.

BURNS, J. C. & PARKES, T. 1967 Peristaltic motion. *J. Fluid Mech.* **29**, 731–43.

CAMPBELL, M. F. 1963 (editor). *Urology*, 3 vols. (second edition). Philadelphia: Saunders.

FUNG, Y. C. & YIH, C. S. 1969 Peristaltic transport. To be published in *J. appl. Mech.*

HANIN, M. 1968 The flow through a channel due to transversely oscillating walls. *Israel J. Technol.* **6**, 67–71.

KIIL, F. 1957 *The Function of the Ureter and Renal Pelvis*. Philadelphia: Saunders.

LATHAM, T. W. 1966 Fluid motions in a peristaltic pump. S.M. Thesis, M.I.T.

MAKSIMOV, A. A. & BLOOM, W. 1957 *A Textbook of Histology* (seventh edition). Philadelphia: Saunders.

NARATH, P. A. 1951 *Renal Pelvis and Ureter*. New York: Grune and Stratton.

SCHLICHTING, H. 1968 *Boundary Layer Theory* (J. Kestin trans., sixth edition). New York: McGraw-Hill.